Track-Before-Detect Algorithm for Faint Moving Objects based on Random Sampling and Consensus

Phan Dao

Air Force Research Laboratory, Space Vehicles

Richard Rast and Waid Schlaegel

AFRL, Directed Energy

Vincent Schmidt

AFRL, Human Effectiveness Directorate

Stephen Gregory

The Boeing Company

Anthony Dentamaro

Institute for Scientific Research, Boston College

ABSTRACT

There are many algorithms developed for tracking and detecting faint moving objects in congested backgrounds. One obvious application is detection of targets in images where each pixel corresponds to the received power in a particular location. In our application, a visible imager operated in stare mode observes geostationary objects as fixed, stars as moving and non-geostationary objects as drifting in the field of view. We would like to achieve high sensitivity detection of the drifters. The ability to improve SNR with "track-before-detect (TBD)" processing, where target information is collected and collated before the detection decision is made, allows respectable performance against dim moving objects. Generally, a TBD algorithm consists of a pre-processing stage that highlights potential targets and a temporal filtering stage. However, the algorithms that have been successfully demonstrated, e.g. Viterbi-based and Bayesian-based, demand formidable processing power and memory. We propose an algorithm that exploits the quasi constant velocity of objects, the predictability of the stellar clutter and the intrinsically low false alarm rate of detecting signature candidates in 3-D, based on an iterative method called "RANdom SAmple Consensus" and one that can run real-time on a typical PC. The technique is tailored for searching objects with small telescopes in stare mode. Our RANSAC-MT (Moving Target) algorithm estimates parameters of a mathematical model (e.g., linear motion) from a set of observed data which contains a significant number of outliers while identifying inliers. In the pre-processing phase, candidate blobs were selected based on morphology and an intensity threshold that would normally generate unacceptable level of false alarms. The RANSAC sampling rejects candidates that conform to the predictable motion of the stars. Data collected with a 17 inch telescope by AFRL/RH and a COTS lens/EM-CCD sensor by the AFRL/RD Satellite Assessment Center is used to assess the performance of the algorithm. In the second application, a visible imager operated in sidereal mode observes geostationary objects as moving, stars as fixed except for field rotation, and non-geostationary objects as drifting. RANSAC-MT is used to detect the drifter. In this set of data, the drifting space object was detected at a distance of 13800 km. The AFRL/RH set of data, collected in the stare mode, contained the signature of two geostationary satellites. The signature of a moving object was simulated and added to the sequence of frames to determine the sensitivity in magnitude. The performance compares well with the more intensive TBD algorithms reported in the literature.

1. INTRODUCTION

One approach to detect moving point source objects is to apply a threshold to the data and to treat those pixels that exceed the threshold as point measurements. This is acceptable if the signal to noise ratio (SNR) is high but becomes impractical for dim objects because setting a low threshold, to warrant sufficient detection probability, produces

false tracks. Track Before Detect (TBD) algorithms that do not rely on pixel value thresholding have been investigated to detect dim moving objects. Davey [Davey 2008] compared the performance of the most representative algorithms. The algorithms in their comparison are the Bayesian estimator for a discrete state space, detailed in Stone's paper [Stone 1999], a Viterbi algorithm [Barniv 1990], the particle filter by Rutten et al. [Rutten 2005] and the Histogram Probabilistic Multi-Hypothesis Tracker [Streit 2000]. Davey et al. showed that at 3dB peak SNR, the algorithms began to show degraded performance and detected the objects at less than 50 percent probability. TBD has been also tackled by Tartakovsky, et al. [Tartakovsky 2010] for both GEO and low earth orbits (LEO). Successful detection with SNR levels down to ¼ has been reported, though we could not confirm if the value reported in Tartakovsky's paper is the same as the peak SNR used in this paper and other references, and we have not been able to reconcile Tartakovsky's performance with previous results. The peak SNR (pSNR) quantifies the intensity at the peak of the object's point spread function relative to the noise floor. The pSNR in dB is typically defined as $20 \log(I/\sigma)$, a function of peak intensity and noise standard deviation σ. Note that the effects of the stellar clutter are not included in this definition. In summary, all the TBD algorithms have been shown to perform well for pSNR down to 3dB.

The RANdom SAmple Consensus for Moving Target (RANSAC-MT) algorithm under development makes use of the assumption that for a range of fields of view and observation times, the apparent motion of the object is quasi-linear. RANSAC-MT takes advantage of the reduced spatial density of quantized and detectable blobs of pixels, in 3-D data to search for the object's linear streak. A sequence of images is acquired with the object appearing in many frames of the sequence. With optical measurements and for decent observational conditions, the clutter is dominated by stars. The frame integration time could be chosen to be long enough so that stars streak across the image in more than one pixel. In a typical scenario, though not essential, the sensor stares at a fixed direction and observes geostationary satellites that appear to be stationary. In this scenario, the objects of interest may drift 0.2 to 3 pixels per frame. The objective is to detect the object with minimum delay, high detection probability and low false alarm rate even for low pSNR. The performance of RANSAC-MT will be documented as minimum detectable pSNR and also as minimum detectable magnitudes for selected systems. Our technique doesn't require intensity thresholding to detect the object; however, it depends on quantization to reduce the amount of information to process and to keep computational latency at practical levels. Similar to the TBD algorithms, the detection is accomplished when the information in all the frames has been processed. It should be pointed out that mainstream TBD algorithms address a wider range of scenarios for objects moving in space as well as in air, while RANSAC-MT is limited to non-maneuvering space objects with apparent linear motion as mentioned above. It's worth mentioning that 3-D matched filter techniques to detect objects traveling through a sequence of noisy images also exploit the assumption of constant velocity, but in a very different manner. Earlier development of RANSAC-MT was focused on data collected with Photon Counting Imagers [Dao 2013]. This paper explores the use of RANSAC-MT with more traditional imagers such as CCDs.

2. DATA COLLECTION

We use two data sets, one collected by the Human Effectiveness Directorate (RH) with the telescope at Wright-Patterson Air Force Base (Figure 1.a) [Shattuck 2012] and the second set collected by the Directed Energy Directorate (RD) at Kirtland Air Force Base with a COTS lens and EM-CCD camera Figure 1.b). The RH telescope is the Planewave 17" CDK equatorially mounted on a Mathis Instruments MI-500 with MI-750 fork arms. That system is used with a SBIG 8300M monochrome camera with 8.3 megapixels (3326 x 2504 pixels). The FOV is 21 x 16 arc-min. We use the RH data set that captured the calibrated signatures of the AMC-18 geostationary satellite the night of October 2, 2013 between UT = 0312 and UT = 0436. The Kirtland system consists of a commercial Advanced Developers Laboratory VFA5095H lens, coupled with a Salvador Imaging SI-VGA60-EM camera. The lens has a 50-millimeter focal length with a focal ratio of 0.95. The diagonal FOV is 9.5 degrees. The data was collected on October 26, 2012, starting at 10:09:10 UTC. The object of interest, SSN 36583 (upper stage for

ASTRA 3B), is at a range of 13865 km and an altitude of 12115 km. The right ascension and declination are 107.587deg and -10.91deg, respectively, at the start.

Figure 1: (a) AFRL/RH 17-inch telescope inside the dome. (b) AFRL/RD EM-CCD based camera

3. RANSAC-MT TECHNIQUE

Before RANSAC-MT can be applied to the data, each frame is processed to enhance object signature while suppressing background noise. A median subtraction filter is used in the pre-processing to suppress spurious noise. We also use morphological filtering to consolidate the groups of signature pixels associated with the object's point spread function. The idea is to represent each blob of relevant pixels by a single point, the blob's centroid. The MATLAB function *bwlabel* efficiently finds and labels the spatially-connected pixels which are brighter than a selected threshold. Objects which are convolved by the point spread function are favorably detected by *bwlabel* while detector's salt and pepper noise, predominantly point-like signature (single pixel), are rejected. The intensity threshold used with the filter is chosen adaptively to curtail the rejection of candidate blobs while maintaining an acceptable total number of blobs to be processed. Currently, processing more than 10^5 blobs cannot be achieved in near real time operation with a COTS PC.

Figure 2 shows the probability distribution functions (PDF) of the intensity of two types of pixel. The first PDF is for the pixel's intensity due to sensor noise and background in the absence of a target. The PDF is a normal distribution with a non-zero mean and standard deviation of 10 (arbitrary value chosen for illustration). The mean is arbitrary because we can vary the zero level. The second PDF represents object's intensity plus background noise.

The average intensity of the object is arbitrarily chosen to be 15 for an SNR of 1.5 in this example. The mode of the second PDF is shifted to the right of the first PDF by 15 a.u. The probability of detection (exceeding the threshold t) is the integral under the PDF curves from t to infinity. The mode of the object's PDF is the mean intensity of the pixel.
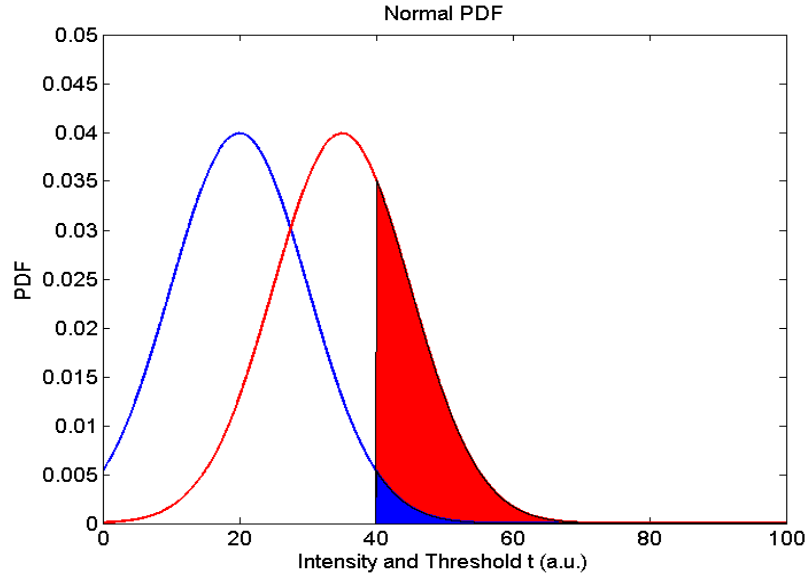

Figure 2. Probability Distribution Functions of pixel intensity. Probability distribution of background's blob intensity (blue) and object's blob intensity (red). In this example, the object's signal is 15 a.u., and the background intensity is distributed as a normal distribution with a Gaussian half-width of 10 a.u. The SNR is 1.5. When the signal is defined as peak intensity, pSNR is 1.5, or 1.76 dB.

For this example, we assume there is a sequence of 100 frames in which the object is present. Using the listed parameters and setting the detection threshold t at 40 a.u. result in a detection probability p=0.023 for background pixels and p=0.31 for target pixels. The probability of surviving the quantization with threshold t is the area under the normalized PDF curve from t to infinity, shown in Figure 2. If the number of possible blobs, a number typically smaller than the number of pixels, is 10^6, and the intensity threshold is set at 40, we have 0.023×10^6 or 2.2×10^4 blobs due to background noise. In addition to those background blobs, we also have a number of object blobs equal to 0.31 times the number of frames in which the object shows up. For 100 frames, the number of object blobs above the threshold is 31. Our objective is to search the streak of object blobs among all the blobs that survive quantization, 31 in this example, using the RANSAC-MT algorithm. The achievable peak SNR (pSNR) is related to the threshold t used with *bwlabel*. A low threshold results in a higher probability for object pixels to survive the *bwlabel* filter but also results in a larger number of background pixels above threshold. Bear in mind that computing requirements limit the number of blobs we can treat with RANSAC-MT in one batch. For this reasons, we will set the threshold adaptively. We will discuss that limitation in detail later. Figure 3 shows the relationship between the threshold value t and the total number of blobs (black curve) and the number of object blobs for two pSNR levels (blue and red.)

In this example, if one uses a threshold of 40, the total number of blobs is 2.2×10^4 and there are 31 object blobs that survive the quantization if the pSNR of that object is 1.5, or 1.78dB. For a 3dB target, the number of object blobs increases to 50. Because RANSAC-MT searches for the streak in 3-D, where the blob density is very low, we will proceed to show the statistical significance of finding as little as 20 blobs lined up on a streak. In 2-D data sets, the expected number of photons on a streak, λ_{2D}, is approximated by $\lambda_{2D} = \frac{B}{D^2} D = \frac{B}{D}$ (1), where B is the number of background blobs in the data set, and the number of resolution cells D can be approximated by the pixel dimension
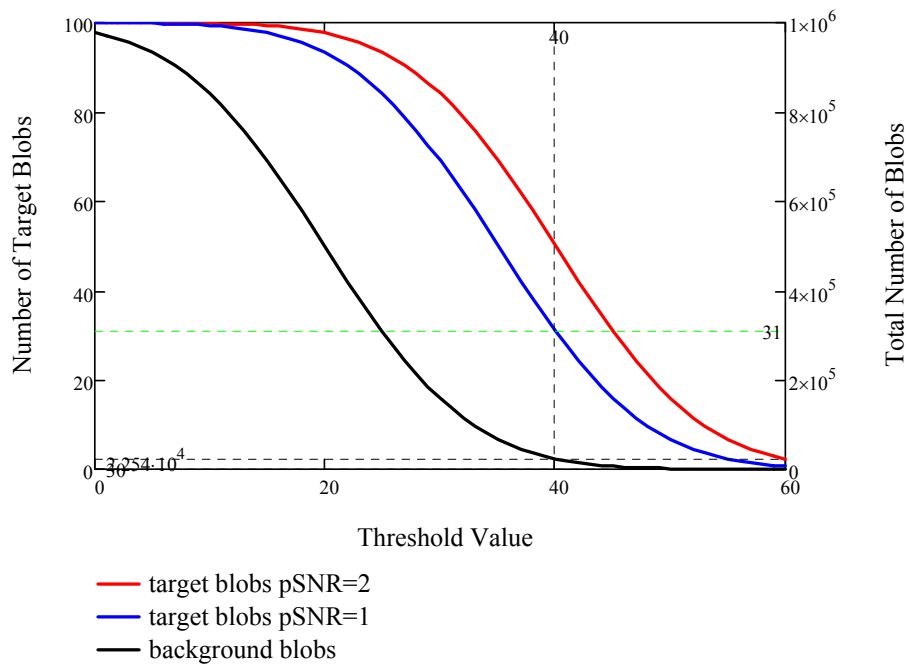
Figure 3. The number of target blobs surviving *bwlabel* pSNR=1 and 2 is plotted against threshold (left vertical axis). The total number of background blobs vs threshold is also shown (right vertical axis).

reduced by a factor determined by the morphological filter *bwlabel*. In a data cube, the number density is reduced by a factor of D or $\lambda_{3D} = \frac{B}{D^2}$ (2) . See [Dao 2013.] The probability P of finding a streak with more than *m* blobs or photons in a data cube of N blobs is estimated by the Poisson distribution or further approximated by a normal distribution with $mean = \lambda_{3D} \ and \ \sigma = \sqrt{\lambda_{3D}}$. We will use the normal distribution to approximate the probability of finding m background blobs.

The number of random streaks the algorithm has to analyze to warrant 90% confidence level that one of them contains m blobs is estimated as $N = \ln(0.9)/P(m)$. The probability of finding one streak with m blobs at 90% and 99% confidence levels is shown in Figure 4. It is interesting to learn that the probability of finding a streak with as little as 18 background blobs among all the possible streaks in the data cube is less than 10^{-3}. Due to the limitation of double precision numbers used in MATLAB, the calculations are limited to a maximum m of 18. In Figure 4, the trend for m < 18 is used to estimate that the probability of finding a 20 blob streak is $\sim 10^{-6}$. Note that the shown estimate of probabilities does not include the stellar blobs. The stars can also form streaks, but their streaks have deterministic direction and length and therefore can be removed in another step of the algorithm. The probability shown in Figure 4 is also interpreted as the false alarm probability for associating an m-blob streak with a moving object. One can conclude that the false alarm rate is 10^{-6} for a 20 blob streak in this case. It is interesting to note that the probability of detecting the streak or the moving object depends on the performance of the algorithm, while the false alarm rate is warranted to remain very low as long as the number of blobs on the discovered streak is higher than 20. It's also important to mention that in real data sets, the object intensity can fluctuate, and there will be many frames for which the object's intensity is near zero. In these cases, the peak intensity used to calculate the limiting pSNR is much higher than the average intensity of the object because of the requirement of having more than 20 object blobs. The limiting pSNR that can be achieved for a fluctuating signal is therefore higher than that of a steady one.

The RANSAC technique we use for the search is based on the research conducted in the field of vision research and LADAR 3D analyses. Fischler published an iterative method to estimate parameters of a mathematical model from a set of observed 3-D data [Fischler 1981]. Based on the principles of Fischler's RANdom SAmple Consensus (RANSAC), we developed an algorithm called RANdom SAmple Consensus –Moving Target (RANSAC-MT) to search for data points that conform to a linear signature model and the constraints due to the point spread function and the pixel format. As with RANSAC, RANSAC-MT is a non-deterministic algorithm that can produce reasonable result only with a certain probability. This probability increases as more iteration is allowed. For

Figure 4. False alarm rate as function of the number of blobs in a streak. At 99% confidence level, the false alarm rate for a streak of 18 blobs is $6x10^{-5}$.

practical purposes, we have to consider the tradeoff between speed and sensitivity. The relationship between the number of iterations T and the desired probability p of finding the streak is as shown $T = \dfrac{\log(1-p)}{\log\left(1-\left(\frac{m}{B}\right)^2\right)}$ (3).

Probability of finding 1 streak with m blobs

90%
99%
trace 3
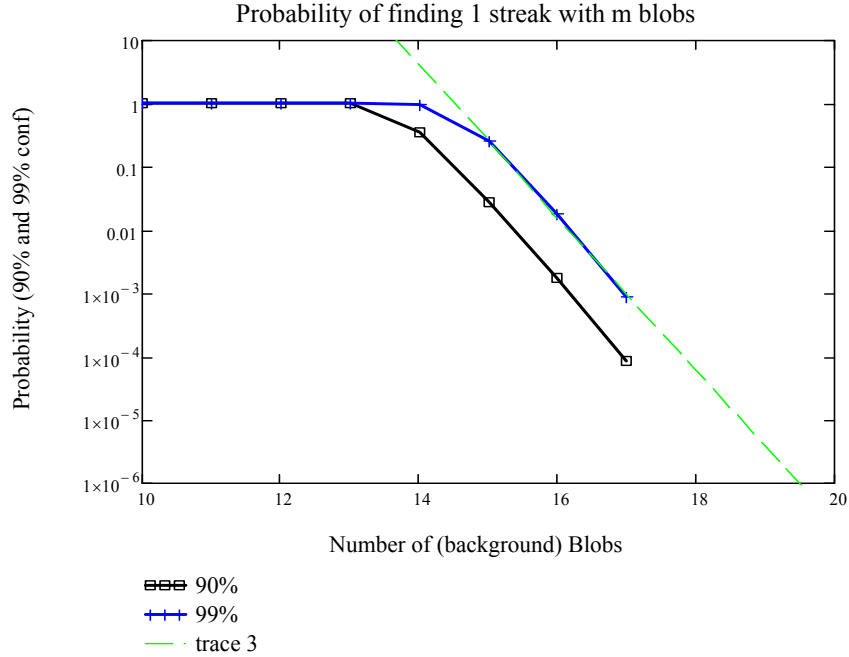
4. ANALYSIS AND RESULTS

Figure 5 shows the estimated (maximum) velocity in pixels per frame for a space object at shown altitude. For optimum operation, the integration time is chosen to keep the displacement to less than 3 pixels between frames. The thick lines show the displacement of the object on an FPA with 1Kx1K pixels covering a field of view of 15 degrees and frame integration time as shown in the legend. The red and blue thin lines correspond to a sensor with a 1 degree FOV. As predicted, displacement increases with integration time. For displacement larger than 5 pixels the object's image becomes a streak with reduced peak intensity relative to that of a stationary object. We would like to keep the integration time small enough to minimize streaking and use RANSAC to process multiple frames. Figure 5 highlights the utility of the algorithm. It can be used to extend the range of altitudes for a moderately wide FOV used to survey deep space or to extend the range of altitudes for a very wide FOV (tens of degrees) sensor covering LEO. The extension is attributed to the ability to exploit a long sequence of frames while keeping the integration time low enough to not be affected by motion. RANSAC-MT is the technique we develop to process a sequences of frames with a moving target (MT). There are two regimes of operations. For LEO-GEO observation with a wide field of view, the frame interval or integration time is kept at 1 to 3 sec to keep the streak length less than 3 pixels. The red thick curve corresponds to 1 sec integration, and the blue thick one for 2.6 sec. Note that the permissible integration time is inversely proportional to displacement on the focal plane array, therefore stationary or nearly stationary objects do not require processing by RANSAC-MT because longer integration time or co-adding frames will also improve the SNR. For GEO observation (brown rectangle), where a small FOV may be required for high sensitivity, the thin blue and red lines describe the object's motion in a 1 degree FOV with 1 and 2.6 sec frame intervals, respectively. We will show that RANSAC-MT can be used in both regimes of FOV to achieve detection. Note that the motion displacement (in pixels), shown in Figure 5 and calculated by assuming the objects are seen at the highest elevation, is a conservative bound of the actual displacement.

With the data set collected with the RH 17-inch telescope, the night of 2014/10/02 UT, we evaluate the performance of RANSAC-MT by testing it using simulated data. Adding the simulated signatures of a drifting object to the observed frames allowed the introduction of object signature with different SNRs. In the sequence of measured frames, the sensor stared at geostationary satellite AMC-18. The magnitude of AMC-18 is determined using standard calibration techniques. Moving object signatures of various intensities and angular velocities are tested. Figure 6 shows the results from one of the runs where the signal strength is set at the lowest level to achieve a probability of detection better than 60%. The blobs are shown in normalized coordinates. In the left data cube; the object's blobs which are retrieved by RANSAC-MT are shown in red. All the blobs have been verified to belong to the simulated streak. The data cube on the right is oriented such that the streak is close to the line of sight, and the object's blobs are encircled by the red ellipse. Figure 7 shows the magnitudes of the geosatellite which is used as the benchmark against which the simulated signature is evaluated. The average magnitude of the satellite is m=12.3 in the data cube. Based on that calibrated source, the minimum detectable magnitude of the moving object is 17.3 when 100 frames spanning 1000 sec are used.

The second data set, which was collected with a wide FOV camera with a 53 mm aperture, captured the signature of SCN 36583 (ARIANE 5 R/B) observed near 146.1 deg. (East of North) azimuth and 38.2 deg. elevation. The rocket body is in a highly elliptical orbit with the apogee at 34694 km. It was observed at a range of 13865.44 km so it was moving in the staring FOV. The solar phase angle is 79.41deg, so one expects the signature of the tumbling body to be flickering. The images did show substantial modulation, and one of the stronger glints was captured in Figure 8. The star we use for calibration is at 141.84 deg. azimuth and 35.4 deg. elevation. The frames were co-added to form 100 composite frames, each 2.6 sec in duration. The 100 frames were analyzed by RANSAC-MT, and the retrieved streak is shown in Figure 8. The number of blobs indicates that the peak intensity is 1.7dB above the noise floor only 40% of the time. The maximum magnitude of the glints (shown on the left of Fig 8) is 8.7[th] magnitude. The average magnitude of the moving object is m_v=10.5.

5. DISCUSSION AND CONCLUSIONS

For wide FOV images, the field is dominated by the clutter of stars. Figure 8 (right) shows a large number of streaks which are nearly vertical (stationary). These are the remaining of the star field after 80-85% of the stellar intensity has been removed in the preprocessor step. While RANSAC-MT can reject the star tracks based on a priori information, the sheer number of blobs can overwhelm the algorithm.

We have demonstrated that for a moderately wide FOV (0.35 x 0.27 deg) and very wide FOV (diagonal 9.5 deg), RANSAC-MT has been effective in detecting a moving object at 1.7 dB above the noise floor. Using the calibration of the stars and that of a geostationary satellite located in the frame, we have been able to estimate that the moving object's limiting magnitude for that 17-inch sensor was mv ~ 17 when the frames are analyzed with RANSAC-MT. In addition, a moving object (ARIANE 5 R/B) was detected in the data collected with a commercial camera coupled to an EM-CCD. The average brightness of the rocket body was estimated to be m_v=10.4.

ACKNOWLEDGEMENTS

REFERENCES

[Davey 2008] S. J. Davey, M. G. Rutten and B. Cheung, *A Comparison of Detection Performance for Several Track-Before-Detect Algorithms*, 2008 11th International Conference on Information Fusion, June 30 2008-July 3 2008, Cologne, Germany.

[Stone 1999] L D Stone, C A Barlow, and T L Corwin, *Bayesian Multiple Target Tracking*, Artech House, 1999.

[Barniv 1990] Y Barniv, *Dynamic programming algorithm for detecting dim moving targets*, Yaakov Bar-Shalom, editor, Multitarget-Multisensor Tracking: Advanced Applications, chapter 4. Artech House, 1990.

[Rutten 2005] M G Rutten, N J Gordon, and S Maskell, *Recursive track-before-detect with target amplitude fluctuations*, IEE Proceedings on Radar, Sonar and Navigation, 152(5):345–352, October 2005.]

[Streit 2000] R L Streit, *Tracking on intensity-modulated data streams*, Technical report 11221, NUWC, Newport, Rhode Island, USA, May 2000.

[Tartakovsky 2010] Tartakovsky, A. G., Brown, A., and Brown, J., Nonstationary EO/IR Clutter Suppression and Dim Object Tracking, Proceedings of the Advanced Maui Optical and Space Surveillance Technologies Conference, held in Wailea, Maui, Hawaii, September 14-17, 2010.

[Dao 2013] Phan Dao, Peter Crabtree, Patrick McNicholl and Tamara Payne, *Blind Search of Faint Moving Objects in 3D Data Sets*, 2013 AMOSTECH proceedings, Wailea, HI, Sept 2013.

[Fischler 1981] Martin A. Fischler and Robert C. Bolles,"Random Sample Consensus", Comm. of the ACM 24 (6), June 1981.

[Shattuck 2012] Shattuck III, J. L., Schmidt, V. A., Campbell, P. (2012) "Installation and Adjustment Procedure for the Portable Pier and PlaneWave CDK-17 Telescope", AFRL-RH-WP-TR-2012-0122.
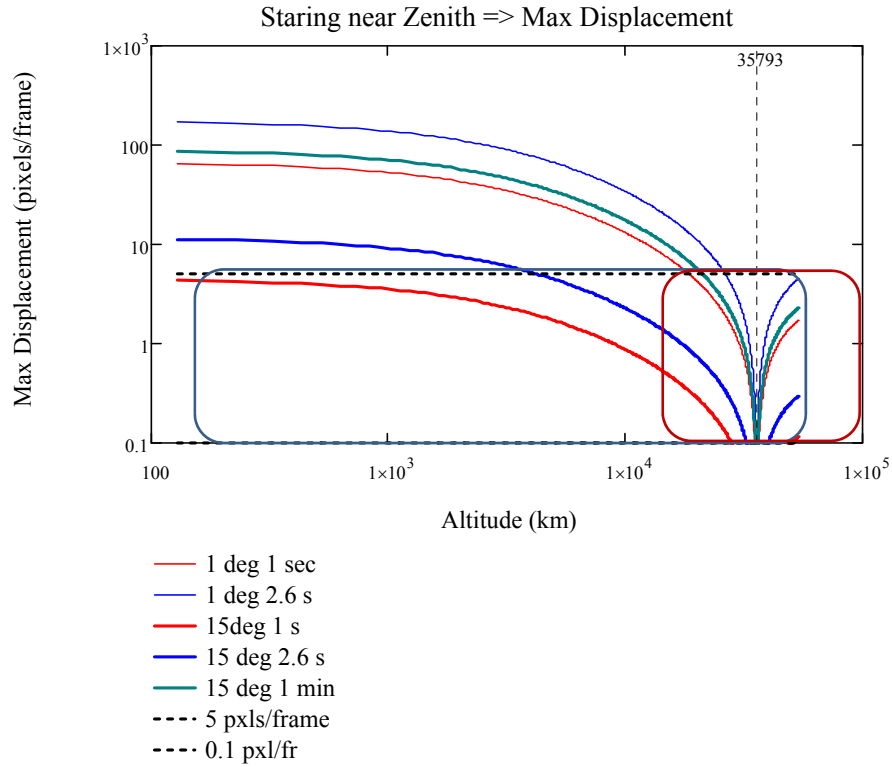
Staring near Zenith => Max Displacement

1×10³   35793

Max Displacement (pixels/frame)

Altitude (km)

— 1 deg 1 sec
— 1 deg 2.6 s
— 15deg 1 s
— 15 deg 2.6 s
— 15 deg 1 min
---- 5 pxls/frame
---- 0.1 pxl/fr

Figure 5. Maximum velocity (pxl/frame) of objects as a function of altitude and FOV.

Found inliers are marked in red

100001 trials
07e-03 s
er pts 23 among 6490 points
3000, Tol=93
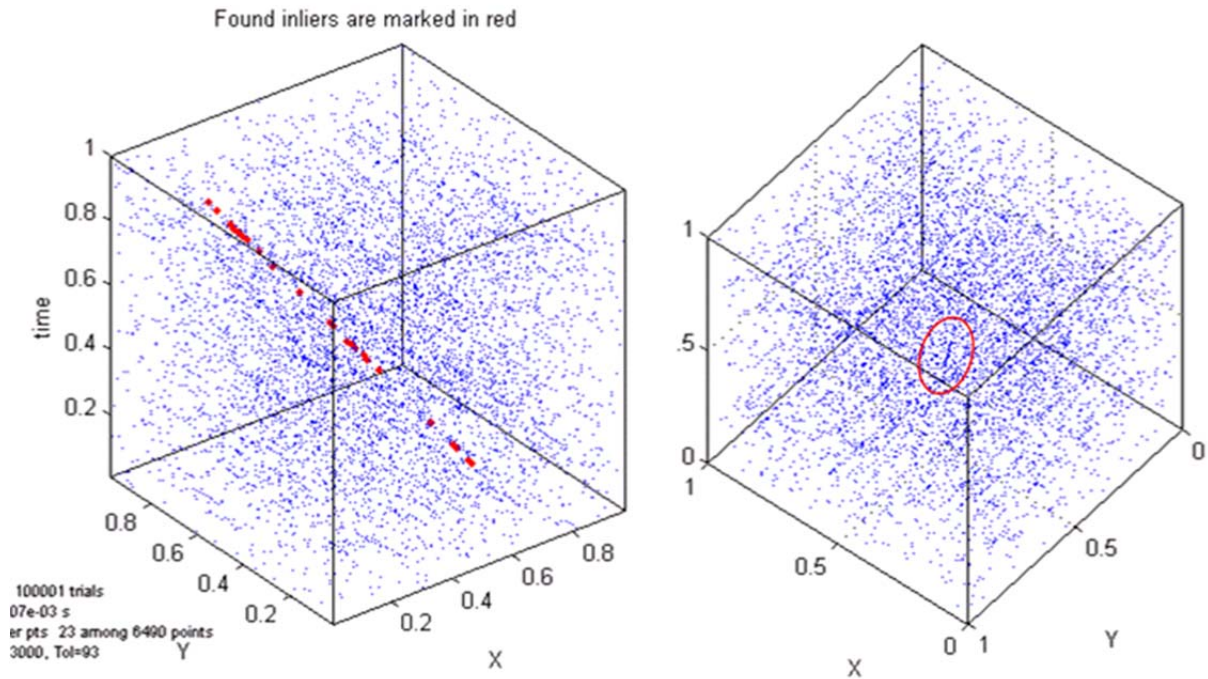
Figure 6. Processing of data set collected by RH and simulated signature of a moving object. The blobs retrieved by RANSAC-MT are highlighted in red in the left data cube. On the right, the same cube is rotated to maximize visibility of the blobs which are encircled in the red ellipse. All positional and temporal coordinates are normalized.
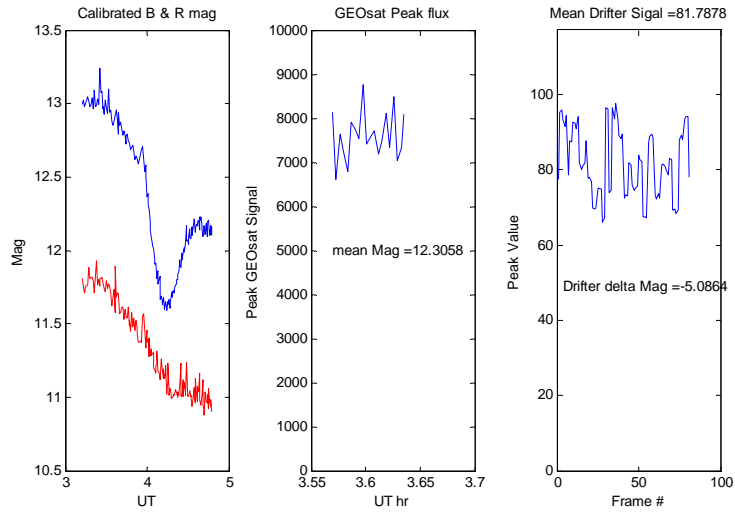
Figure 7. Magnitude of GEOsat and that of simulated moving object. In comparison to the calibrated magnitude of the satellite, the mover's magnitude is about 17[th.]
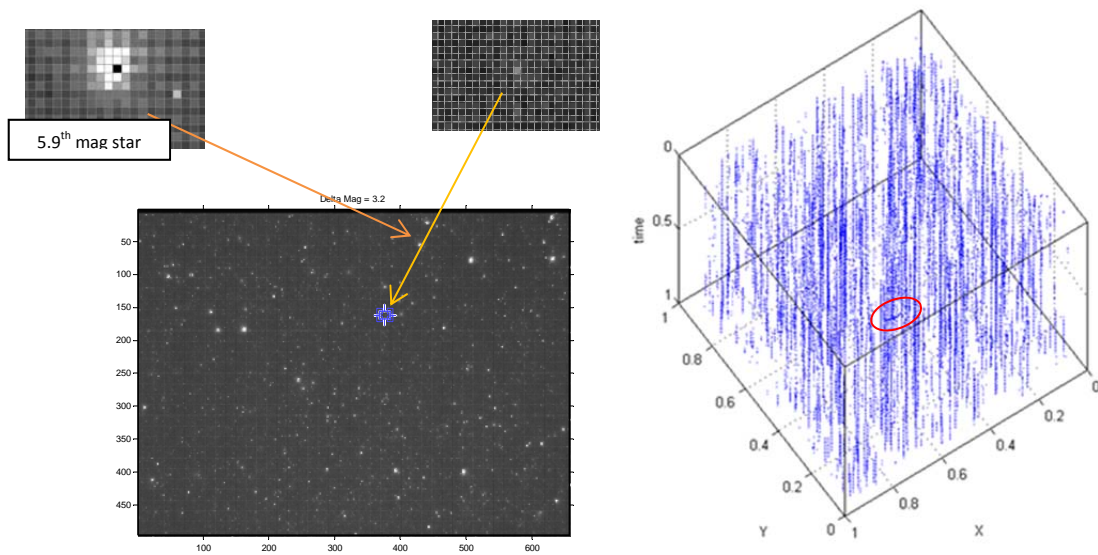

Figure 8. Analysis of data collected at KAFB showing that RANSAC-MT can detect SCN 36583 (ARIANE 5 R/B) in a sequence of frames collected with a COTS camera and lens combination. On the left panel, the image shows a glint (mv=9.1) from the object and the star used for calibration. The retrieved blobs are encircled in the red ellipse. Note that even with 85% of the stellar intensity removed, the data cube is still dominated by the quasi-vertical streaks of the stellar background. They are however rejected by the algorithm.